Journal of Materials Chemistry A

Toward High Energy-density and Long Cycling-lifespan Lithium Ion Capacitor: A 3D Carbon Modified Low-potential Li2TiSiO5 Anode Coupled with A Lignin-derived Activated Carbon Cathode

Journal:	*Journal of Materials Chemistry A*
Manuscript ID	TA-ART-12-2018-012000.R2
Article Type:	Paper
Date Submitted by the Author:	19-Feb-2019
Complete List of Authors:	Jin, Liming; Tongji University, Clean Energy Automotive Engineering Center and School of Automotive Studies Gong, Ruiqi; Tongji University zhang, weichao; c. State Key Lab of Organic-Inorganic Composites, College of Chemical Engineering, College of Energy, Beijing University of Chemical Technology xiang, yue; Tongji University Zheng, Junsheng; Tongji Unviersity, Clean Energy Automotive Engineering Center ; Florida State University , Department of Electrical and Computer Engineering ZH, Xiang; c. State Key Lab of Organic-Inorganic Composites, College of Chemical Engineering, College of Energy, Beijing University of Chemical Technology Zhang, Cunman; Clean Energy Automotive Engineering Center, Xia, Yong-Yao; Institute of New Energy, Department of Chemistry Zheng, Jim; Florida State University, Electrical and Computer Engineering

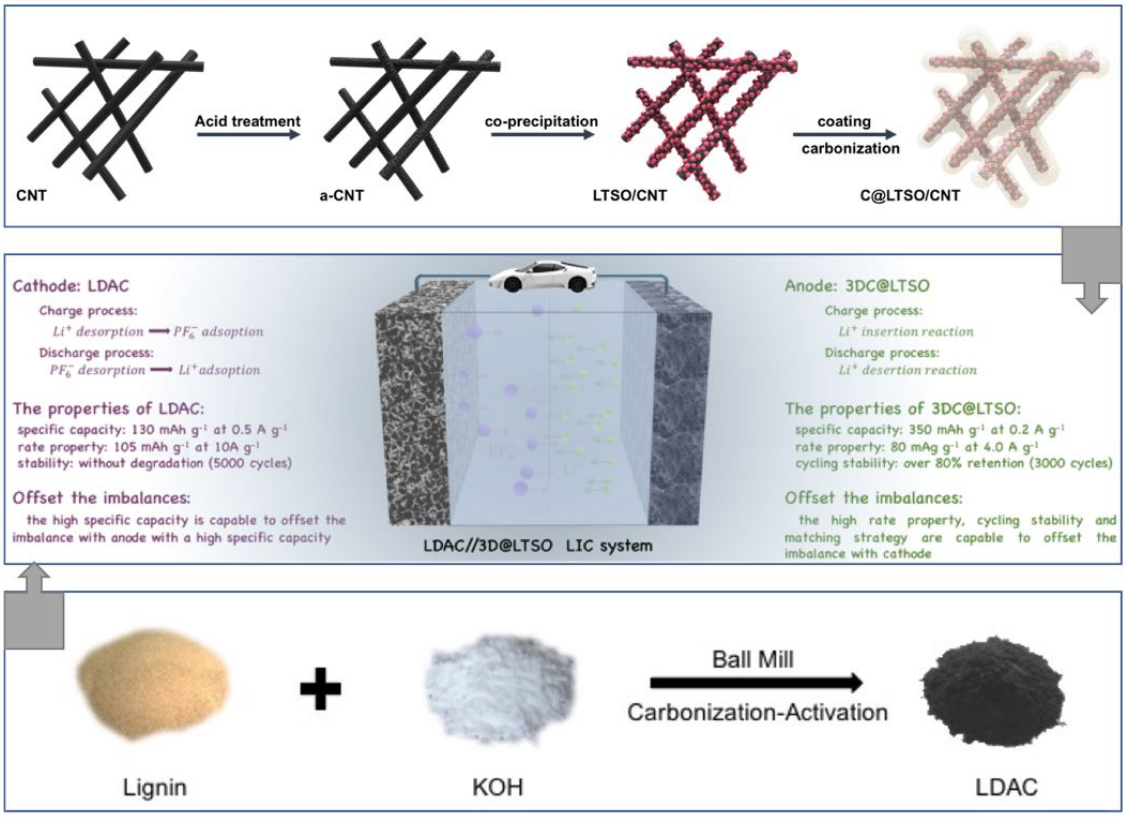
CNT
Acid treatment
a-CNT
co-precipitation
LTSO/CNT
coating
carbonization
C@LTSO/CNT
Cathode: LDAC
Charge process:
Li+ desorption → PF6- adsoption
Discharge process:
PF6- desorption → Li+adsoption
The properties of LDAC:
specific capacity: 130 mAh g-1 at 0.5 A g-1
rate property: 105 mAh g-1 at 10A g-1
stability: without degradation (5000 cycles)
Offset the imbalances:
the high specific capacity is capable to offset the imbalance with anode with a high specific capacity
LDAC//3D@LTSO LIC system
Anode: 3DC@LTSO
Charge process:
Li+ insertion reaction
Discharge process:
Li+ desertion reaction
The properties of 3DC@LTSO:
specific capacity: 350 mAh g-1 at 0.2 A g-1
rate property: 80 mAg g-1 at 4.0 A g-1
cycling stability: over 80% retention (3000 cycles)
Offset the imbalances:
the high rate property, cycling stability and matching strategy are capable to offset the imbalance with cathode
Lignin
KOH
Ball Mill
Carbonization-Activation
LDAC

Journal of Materials Chemistry A

ARTICLE

Toward High Energy-density and Long Cycling-lifespan Lithium Ion Capacitor: A 3D Carbon Modified Low-potential Li_2TiSiO_5 Anode Coupled with A Lignin-derived Activated Carbon Cathode

rReceived 00th January 20xx,
Accepted 00th January 20xx

DOI: 10.1039/x0xx00000x

www.rsc.org/

Liming Jin,[a,b] Ruiqi Gong,[a] Weichao Zhang,[c] Yue Xiang,[a] Junsheng Zheng,[a,*] Zhonghua Xiang,[c,*] Cunman Zhang,[a] Yongyao Xia,[d] and Jim P. Zheng [a,b,*]

Lithium ion capacitor (LIC), which can bridge the gap between lithium ion battery and supercapacitor by combining the merits of the two systems, is thus considered as one of the most promising energy storage devices. However, the imbalances in specific capacity, high-rate behavior, and long cycling lifespan between the two electrodes make it a challenge to develop LICs with high energy density at high power density output along with long cycle life. Herein, a LIC consisted of a three-dimensional carbon modified LTSO (3DC@LTSO) anode and a lignin-derived activated carbon (LDAC) cathode is designed and fabricated. These two electrode materials with desirable electrochemical properties will much favorably offset the imbalances between two electrodes. Moreover, a novel electrode-matching strategic approach, which will further offset the imbalance between two electrodes, is developed. Thereby, the assembled LDAC//3DC@LTSO LIC cell shows a high energy density of 115.3 Wh kg^{-1} at 163.5 W kg^{-1} and a high power density of 6,560 W kg^{-1} at 60 Wh kg^{-1}, coupled with an excellent cycling lifespan of 90% capacity retention after 6,000 cycles at the current density of 2.0 A g^{-1}. These completive results are impressive in terms of pushing high energy density and long cycling lifespan LICs.

Introduction

With the increasing demands for large-scale grid storages, electric vehicles, hybrid electric vehicles as well as consumer electronic devices, the energy storage devices are required to provide both high energy and large power requirements as well as long cycle life in future energy storage systems.[1,2] In the past several decades, lithium ion batteries (LIBs) and supercapacitors (SCs) are two most promising energy storage devices, and a significant volume of researches have been devoted to improving their performance.[3–6] Due to the distinct charge storage mechanisms, LIBs and SCs show complementary energy storage behaviors. For instance, LIBs deliver high energy density (150~250 Wh kg^{-1}) by utilizing Faradic reactions throughout the active materials.[7,8] However, this energy storage mechanism of LIBs results in low power density (<1,000 W kg^{-1}) and poor cycling life (<1,000 cycles) due to the sluggish solid-state ion diffusion in bulk electrodes and the accompanying volumetric strain. Conversely, SCs can provide high power density (>10 kW kg^{-1}) and long cycling life (>100,000 cycles), while the limited charge accumulation leads to low energy density (<10 Wh kg^{-1}).[9,10] Therefore, it is highly desirable to develop an energy storage device by combining the advantages of both LIBs and SCs.

Recently, lithium ion capacitors (LICs) have been proposed as a new generation of hybrid device, which can bridge the gap between LIBs and SCs by combining the merits of the two systems.[11,12] Generally, LIC is consisted of a high energy LIB-type anode, a high power SC-type cathode and a Li salt containing organic electrolyte. LICs worked with cation and anion adsorbing or desorbing onto/from the positive electrode surface and lithium ion intercalating or de-intercalating into/from the bulk of the negative electrode simultaneously. The combination of the faradic intercalation and non-faradic surface reaction provided an opportunity to achieve both high energy and power density, as well as long cycling life.[11,12] However, due to the imbalances in specific capacity, high rate behavior, and long cycling lifespan between the two electrodes, it remained a challenge to develop LICs with high energy density at large power density along with long cycle life. Despite great progress in recent years, it was not satisfied that the high energy densities (30 ~ 90 Wh kg^{-1}) found in most of these reports were always at the cost of the power performance (< 3 kW kg^{-1}).[13]

Based on the above considerations, the key to improved performance of LICs was to couple appropriate anode and cathode materials to offset the imbalance in specific capacity, high rate behavior, and long cycling lifespan. According to the charge-discharge principles of LICs,[12] the merits of an ideal anode for LICs

[a] Clean Energy Automotive Engineering Center, School of automotive studies, Tongji University (Jiading Campus), 4800 Caoan Road, Shanghai 201804, China; E-mail: jszheng@tongji.edu.cn (J.S. Zheng), zheng@eng.fsu.edu (J.P. Zheng)Address here.
[b] Department of Electrical and Computer Engineering, Florida A&M University-Florida State University College of Engineering, FL 32304, USA;
[c] State Key Lab of Organic-Inorganic Composites, College of Chemical Engineering, College of Energy, Beijing University of Chemical Technology, Beijing 100029, China; Email: xiangzh@mail.buct.edu.cn (Z.H. Xiang)
[d] Department of Chemistry and Shanghai Key Laboratory of Molecular Catalysis and Innovative Materials, Institute of New Energy, Collaborative Innovation Center of Chemistry for Energy Materials (iChEM), Fudan University, Shanghai 200433, China.

† Footnotes relating to the title and/or authors should appear here.
Electronic Supplementary Information (ESI) available: [details of any supplementary information available should be included here]. See DOI: 10.1039/x0xx00000x

should include: (*a*) suitable voltage plateau and high specific capacity, which enable higher energy density of LIC devices when pairing cathode; (*b*) desirable rate capability and excellent cycling stability, which offset the imbalance in high rate behavior and long cycling lifespan with cathode. On the other hand, the cathode capacity should be radically improved to offset the imbalance in specific capacity with anode, which usually shows relatively high capacity.[14,15]

Among a myriad of anode materials (e.g. graphite,[16,17] $Li_4Ti_5O_{12}$,[18–20] Fe_3O_4,[21] Si,[22] Li_3VO_4[23,24]), the spinel structured $Li_4Ti_5O_{12}$ (LTO) has attached tremendous attention in the past decades. LTO with three-dimensional (3D) lithium diffusion structure exhibited the negligible volume change during the lithiation/de-lithiation process. Meanwhile, the relatively flat discharge plateau endowed LTO with excellent cycling stability. By developing various hierarchically nanostructured LTO or carbonaceous LTO composites, a series of LTO composite materials with excellent power density were achieved and used as anode materials for high power and durable LICs.[20] However, the high discharge plateau (~1.55 V) as well as low specific capacity (~175 mAh g^{-1}) seriously decreased the output voltage and hence reduced the energy density of LICs, largely weakening their application potential.[18–20]

Recently, another novel Ti-based anode material Li_2TiSiO_5 (LTSO), with an ultralow charge and discharge plateau (~0.28 V) and a relatively large theoretical capacity (>315 mAh g^{-1}), was proposed.[25,26] LTSO was capable to overcome the intrinsic defects of LTO (high discharge plateau and low specific capacity) in a certain degree as well as performing superior cycling durability. However, similar to the physical properties of LTO, LTSO still suffered from inferior rate performance due to the intrinsic poor electronic and ionic conductivities.[25] After improving its conductivities, LTSO was expected to deliver a low discharge plateau, a high specific capacity, a considerable high rate performance as well as a durable lifespan, simultaneously, so that it could be a desirable anode material for LIC with the all desirable merits.[26]

On the other hands, among various cathode materials (e.g. CNT,[27] graphene,[28,29] porous carbon[30,31]), biomass-derived activated carbon (BDAC)[14,15] were attracting more and more attention as electrode materials for energy storage devices due to their tuneable chemical/physical properties, environmentally friendly features, and high economic value. Particularly, BDAC with a high specific surface area and abundant porosity have been successfully synthesized and thus was suitable to be used as cathode materials for LIC due to its excellent capacitance properties.[14,15] In this context, lignin, nature's second largest organism, with the features of low price, easiness to collect from industrial wastewater as well as to extract aromatic compounds,[32,33] was thus considered as one of superior precursors for carbonization. The preparation methods from lignin to BDAC revealed strong feasibility, economy, and environmental friendliness.

Based on all above considerations, herein, we designed and fabricated a three-dimensional carbon modified LTSO (3DC@LTSO) anode and a lignin-derived activated carbon (LDAC) cathode for high energy density LIC. The unique 3DC@LTSO composite was obtained by co-precipitation reaction and calcinations process. 3D carbon structure with interlaced electron and ion diffusion channels enables LTSO a large Li-ion storage capacity, an acceptable charge and discharge rate as well as a stable life durability within a low working window from 0.005 to 2.0 V (vs. Li/Li^+), satisfying the demands of LICs anode. LDAC was synthesized by a directly carbonization-activation process. The LDAC was capable to deliver a high specific capacitance due to its special structures of a 3D porous network, abundant porosity and a high specific surface area (2,808 $m^2 g^{-1}$). As expectedly, these two desirable electrode materials would much favorably offset the imbalances in specific capacity and high-rate performance between two electrodes. Moreover, a novel electrode-matching strategic approach, which was capable to further offset the imbalance between two electrodes, was proposed and applied into this system. Thereby, the assembled LDAC//3DC@LTSO LIC cell showed a high energy density of 115.3 Wh kg^{-1} at 163.5 W kg^{-1} and a high-power density of 6,560 W kg^{-1} at 60 Wh kg^{-1}, coupled with an excellent cycling lifespan of 90% capacity retention after 6,000 cycles at the current density of 2.0 A g^{-1}. These results are promising in terms of pushing high energy-density and long-cycling lifespan LIC by tailoring the nanostructures of both electrodes and optimizing the LIC performance.

Experimental

Preparation of LTSO and 3DC@LTSO: The pristine materials tetrabutyl titanate (A.R.), tetraethyl orthosilicate (A.R.), lithium hydrate (A.R.) and glucose (A.R.) were selected for this synthesis from Sinopharm Chemical Reagent Co.,Ltd without additional treatment. The tetrabutyl titanate and tetraethyl orthosilicate were dissolved in ethanol (solution A) with stoichiometry of Ti and Si, and the lithium hydrate (solution B) and glucose (solution C) were dissolved in deionized water respectively. The Li_2TiSiO_5 was synthesized by co-precipitation process, i.e. the solution A was dripped into solution B slowly and the white suspension (solution D) was transferred into rotary evaporation to obtain white production. After that, the production underwent calcination at the high temperature at 900 °C with the atmosphere of N_2 for 8 hours and the LTSO can be obtained. As a reference, the 3DC@LTSO needed to add CNT into solution B, following dripping solution C into solution D before rotary evaporation.

Preparation of lignin-derived activated carbon: The lignin was extracted from pulping waste liquor and dried in oven. The KOH was selected as activating agent to mix with lignin with a ratio of 1.5:1 and the mixture was ground in a grinder for 6 h. After grinding, the mixture was transferred into tube furnace to calcine at an atmosphere of N_2. The mixture was heated with a rate of 3 ˚C min^{-1} to 450˚C and insulated for 2 h for carbonization process. Further, the mixture was heated with a rate of 5 ˚C min^{-1} to 800˚C and insulated for 1.5 h for activation process. After activation, the mixture was dripped washing by dilute hydrochloric acid and DI water until pH reached 7. After drying, the production of LDAC was finally obtained.

Journal of Materials Chemistry A

ARTICLE

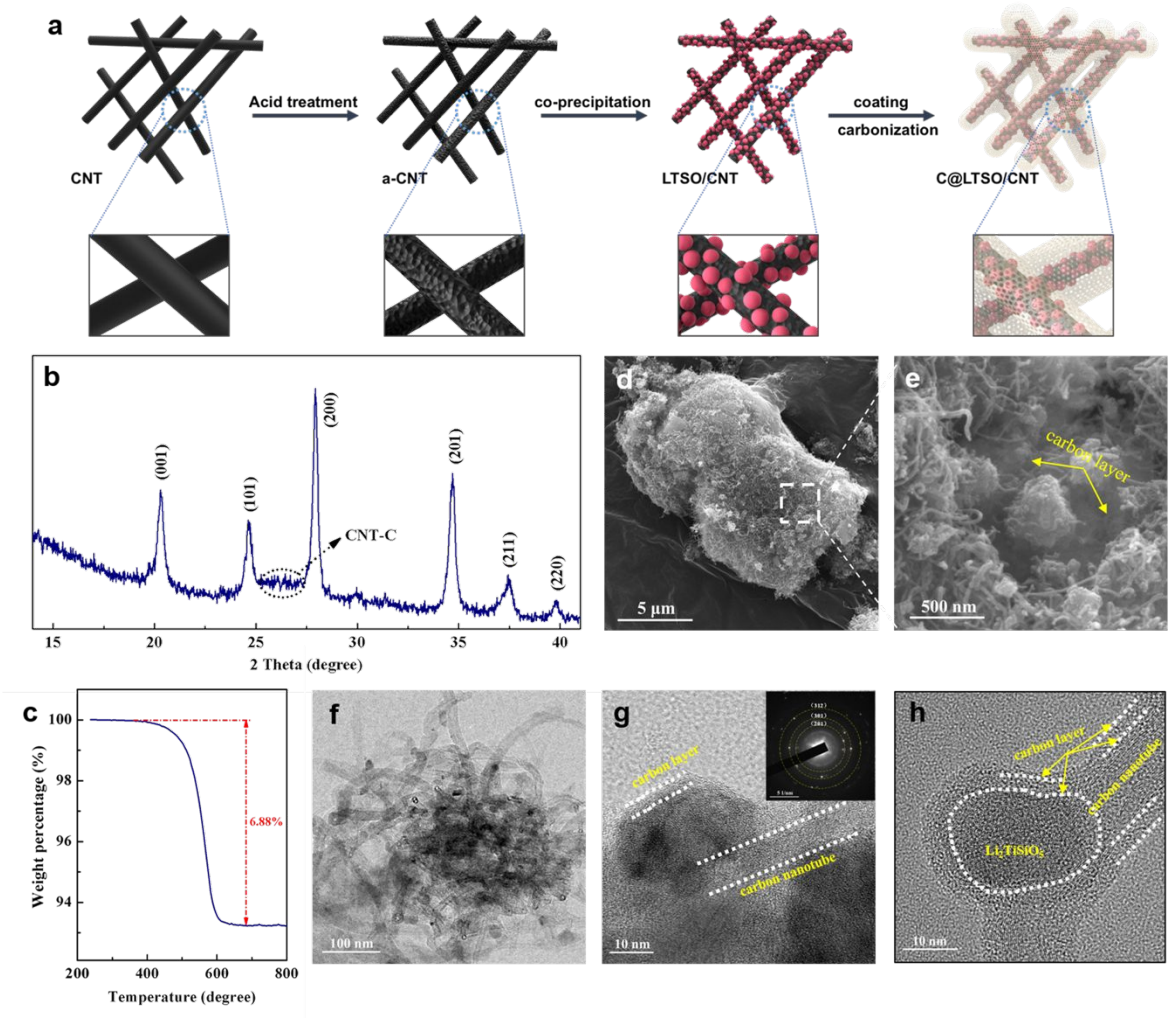

Figure 1. (a) Synthesis procedures schemes; (b) XRD; (c) TGA; (d-e) FESEM and (f-h)TEM of 3DC@LTSO composite material.

Pre-lithiation process: The pre-lithiation process was realized by discharge in a half cell configuration, in which the cell was assembled with a 3DC@LTSO as cathode, a Li foil as counter electrode in an organic electrolyte (1M $LiPF_6$ in EC:DMC) . This pre-lithiation cell was charged and discharged at a rate of 0.2 A g^{-1} for 10 cycles. The last discharge was terminated with a cut-off potential of 0.365 V to achieve pre-lithiation.

Materials characterization: The structure was identified by X-ray diffraction (XRD), with Cu Kα radiation (λ=1.5406 Å) (X'pert PRO PANalytical B.V.). Chemical compositions were analyzed using the X-ray photoelectron spectroscopy (XPS) technique incorporating a 165 mm hemispherical electron energy analyzer, and all spectra were referenced to C 1s at 284.6 eV to correct the peaks. Thermal gravimetric analysis (TGA) was conducted in air from room temperature up to 1,000 ˚C at a heating rate of 10 ˚C min^{-1} using a mettle Toledo TGA/DSC1 STARe System (Metter Toledo, USA & Switzerland). The morphologies and microstructure were observed through field emission scanning electron microscopy (FESEM, Zeiss Ultra 55) at 5 kV, JEOL 1010 transmission electron microscope (TEM), and FEI Tecnai 20 high-resolution (HRTEM).

Electrochemical evaluations: The 3DC@LTSO electrodes and LDAC electrodes were prepared by a coating method. The slurry composed of active materials (80 wt%), super P (10 wt%) and PVDF (10 wt%) was coated on Cu/Al foil. After drying overnight, the electrodes were

obtained. The mass loading of 3DC@LTSO was about 1.0 mg cm^{-2} and the mass loading of LDAC was about 1.0~4.0 mg cm^{-2}. The coin cell (CR2032) was fabricated in an Ar filled glove box, with LDAC electrode as cathode and 3DC@LTSO electrode as anode (a lithium foil was used as a counter electrode when assembling the half-cell,) a microporous polypropylene film (Celgard 2400) as the separator, and electrolyte composed of $LiPF_6$ in DMC and EC with the volume ratio of 1:1. Cyclic voltammetry (CV) profiles were recorded from different voltages at various scan rates, and the galvanostatic charge and discharge tests were conducted using a multi-channel battery tester. All electrochemical measurements were conducted at 25°C. The specific capacity q, energy density E, and power density P of LIC can be calculated following the equations: [34]

$$q = \frac{It}{m} \quad (1)$$

$$E = \frac{1}{2} q (V_{max} + V_{min}) \quad (2)$$

$$P = \frac{E}{t} \quad (3)$$

where *I* stands for the constant current, *t* is the discharge time, *m* is the total mass of cathode and anode while V_{max} and V_{min} are the voltages at the beginning and the end of the discharge procedure.

Results and discussion

The anode material: 3DC@LTSO

The preparation procedures of 3DC@LTSO were illustrated in Figure 1a. In brief, the Li^+ cation was firstly dispersed and adsorbed onto the outside surface of CNT, which was negatively charged by electrostatic interaction. After that, with the addition of tetrabutyl titanate and tetraethyl orthosilicate into solution, the hydrolysis products were immediately anchored on the surface of CNT through a fast co-precipitation reaction between Li^+ and tetrabutyl titanate as well as Li^+ and tetraethyl orthosilicate. During the following rotary evaporation, the LTSO precursor was grown and anchored into porous microspheres following a "nucleation-growth" mechanism with CNT simultaneously embedded in. During this process, the CNT as a dispersing agent would effectively restrain the agglomerations of LTSO precursor for smaller size of LTSO products. Concomitantly, the glucose was polymerized and coated on the surface of LTSO precursor particle and CNT to achieve encapsulation process as well as interacting CNT with CNT to form a 3D structure.[35,36] After carbonization, the LTSO precursor turned into LTSO particles and the glucose resin was carbonized into particle porous amorphous carbon to form 3D carbon network, thus, the 3DC@LTSO composite was finally obtained.[37]

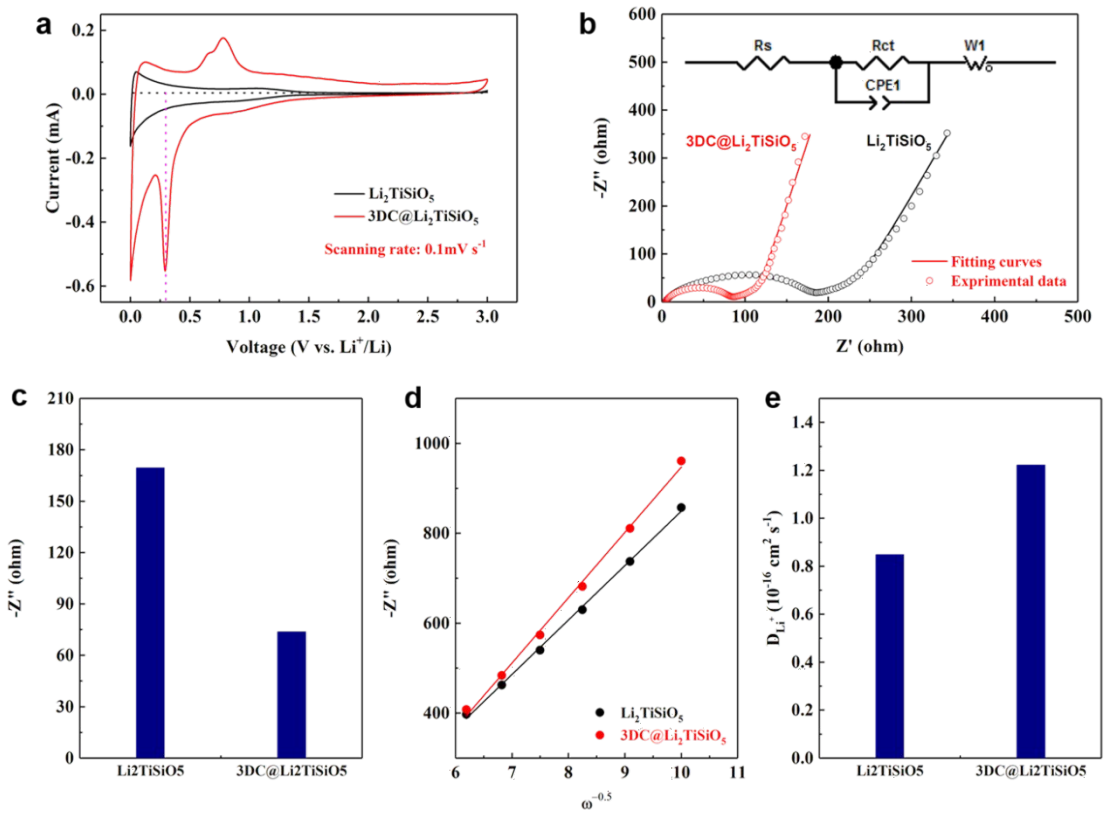

Figure 2. (a) CV; (b) EIS; (c-e) quantitative electron transfer and ion diffusion impedance of LTSO and 3DC@LTSO electrodes.

Journal of Materials Chemistry A

ARTICLE

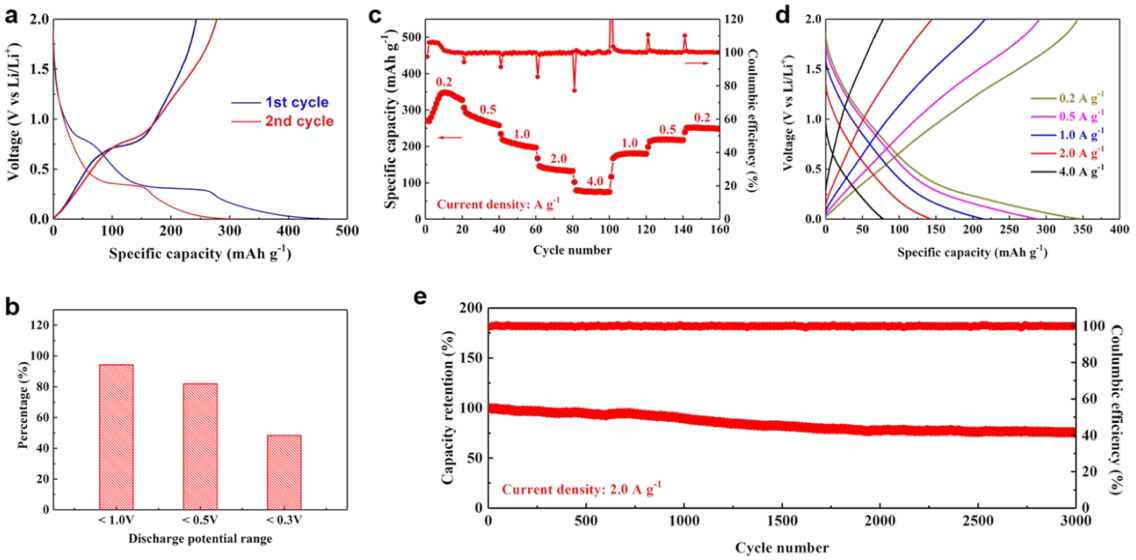

Figure 3. (a) Charge-discharge profile; (b) Potential range distribution; (c) multi-rate performance; (d) multi-rate charge-discharge profiles; (e) long cycling stability of 3DC@LTSO electrode material.

From the structural characterization of XRD (Figure 1b), the diffraction peaks at 20 °, 24.5 °, 28 °, 34.5 °, 37 °, and 39.5 ° were ascribed to (001), (101), (200), (201), (211), (220) crystal planes of LTSO, respectively.[25] The diffraction peaks at a range of 25 °-27 ° were ascribed to the 3D carbon, i.e. CNT and carbon layer.[37] There were no other peaks observed, indicating the excellent purity of 3DC@LTSO composite materials. The Raman Spectrums detected the ID and IG of carbon as shown in Figure S1, further demonstrating the existence of carbon in 3DC@LTSO composite. The TGA was further conducted to determine the carbon content, which was about 6.88 % as showed in Figure 1c.

The structures and morphologies of the as-synthesized pure LTSO and 3DC@LTSO composite were further investigated by FESEM. From the low magnification FESEM image (Figure 1d and Figure S2), we can find that the LTSO was trapped in carbon matrix, and there is no large particle of LTSO observed in 3DC@LTSO composite unlike pure LTSO, indicating reduced particle size. High magnification FESEM images (Figure 1e) showed detailed structure of 3DC@LTSO composite, and it could be found that the LTSO particles and CNT are covered by a thin carbon layer. The transmission electron microscopy (TEM) was also carried out to illustrate the structures (Figure 1f-1g). It could be observed that the LTSO particle with the diameter of ~10 nm anchored onto the surface of CNT, and they were covered by carbon layer to form 3D structure in agreement with the result of FESEM, which would largely boost the electron transfer. Meanwhile, the displayed structures have interconnected morphology, in which a small specific surface area of 62.5 m^2 g^{-1} was associated with a hierarchical pore size from 1-100 nm (Figure S3a-S3b) for fast ion diffusion. These results strongly manifested that LTSO particles with a small particle size and this composite with 3D structure along with hierarchical pores (Figure 1h) would result in high electron transfer and ion diffusion of inherent LTSO particles and 3DC@LTSO composite materials during charging for better high rate performance.

The electron transfer and ion diffusion properties were further detailed demonstrated by CV for pure LTSO and 3DC@LTSO (Figure 2). CV was capable to evaluate the ionic kinetics features (Figure 2a). The CV test was carried with the scanning rate of 0.1 mV s^{-1} at the potential range of 0.005 to 3.0 V for LTSO and 3DC@LTSO, respectively. The curves revealed the reduction peak of 3DC@LTSO was approximately at 0.28 V during discharge process, consistent with previous reports, [25,26] while a higher peak at nearly 0.6 V could be attributed to the formation of solid electrolyte interface (SEI) during the first discharge process. In contrast, there was no discharge peak at 0.28 V for LTSO, which probably resulted from the poor electronic transfer coefficient. Moreover, the redox peak profile of 3DC@LTSO was sharp and symmetric, indicating the redox kinetics of 3DC@LTSO with much improvement in comparison with LTSO. In addition, the anodic and cathodic peak currents (I_p) of the 3DC@LTSO were higher than those of LTSO. Thus, during charge and discharge process, it could be conducted relatively

Journal of Materials Chemistry A

ARTICLE

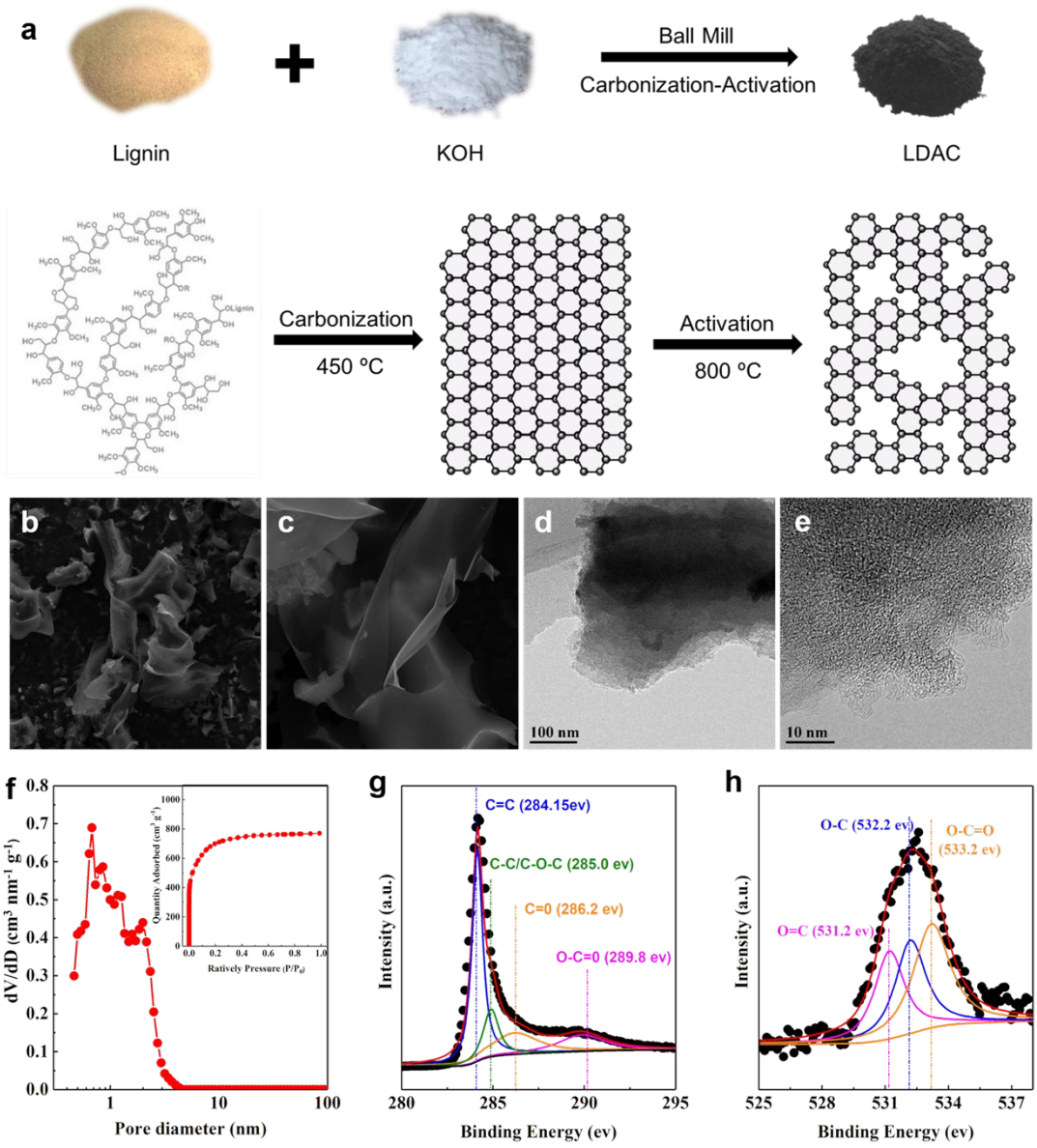

Figure 4. (a) the scheme of synthesis process of LDAC; (b-c) FESEM images; (d-e) TEM images; (f) Pore size distribution (inset is N_2 adsorption and desorption isothermal); (g) C1s spectrum and (h) O1s spectrum of LDAC.

qualitatively that 3DC@LTSO showed larger Li^+ diffusion coefficient (D_{Li}) according to Randles Sevcik formula (S5), in which D_{Li} is proportional to $I_p^{-1/2}$. [37]

Electrochemical impedance spectroscopy (EIS) was also adopted to evaluate the electronic and ionic conductivities of these two samples (Figure 2b-2e) and all the samples were conducted at open circuit potential. For quantificational investigation of electronic and ionic conductivity features, a simplified equivalent circuit was used (inset of Figure 2b). After modifications, the charge transfer resistance (R_{ct}) sharply decreased from 169.5 Ohm to 73.78 Ohm (Figure 2c), arising from the improved electronic conductivity of 3D carbon network structure. The ionic diffusion co-efficient at open circuit could be obtained from the slanted line in the Warburg region by following equation (details in S6):[37,38]

$$D_{Li}^{+}=R^2T^2/2A^2n^4F^4C_0^2\sigma^2 \quad (4)$$

Journal of Materials Chemistry A

ARTICLE

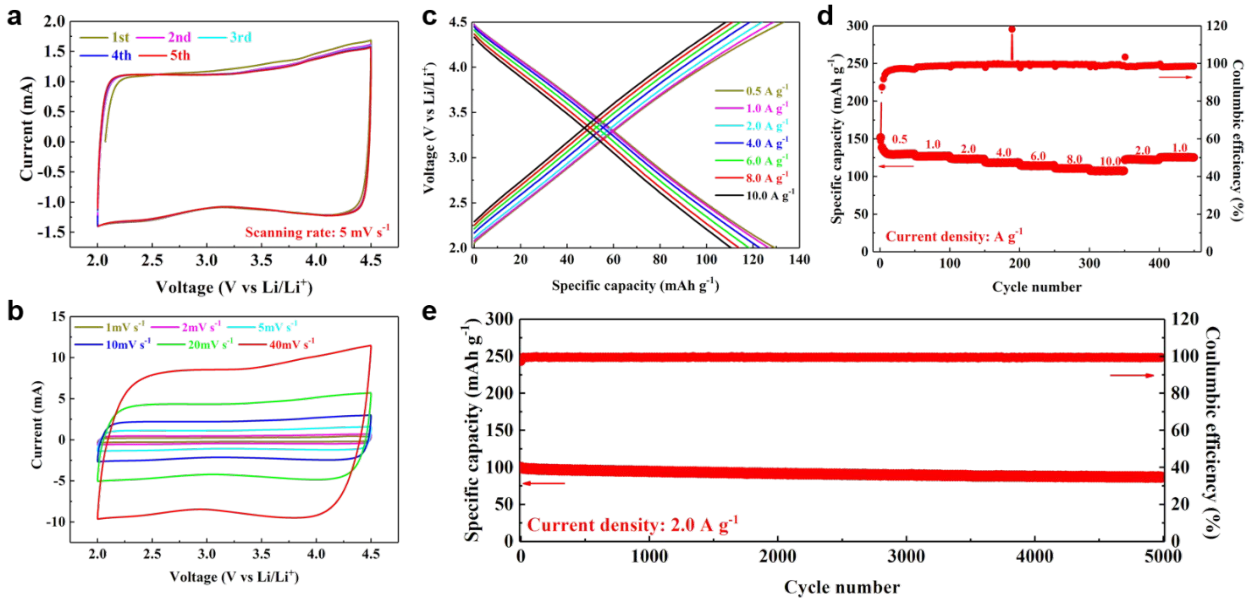

Figure 5. (a-b) CVs; (c) Charge-discharge profile; (d) multi-rate performance; (e) Long term cycling stability of LDAC electrode.

Where σ is the Warburg factor associated with Z_{Re} ($Z_{Re} \infty \sigma\omega^{-1/2}$). Figure 2d displayed the linear fitting relation plot between Z_{Re} and the reciprocal square root of the angular frequency ω. Furthermore, the D_{Li}^+ of these samples were calculated to be 8.49×10^{-17} and 1.222×10^{-16} cm^2 s^{-1} of LTSO and 3DC@LTSO, respectively, suggesting an enhanced ionic transport.

After modification, the electronic and ionic conductivities of 3DC@LTSO were improved as demonstrated above. Thus, the electrochemical properties of 3DC@LTSO were symmetrically investigated by half cells, which were fabricated using coin cells with lithium metal foil as the counter and reference electrodes. The charge-discharge profiles of the first and second cycles were obtained by galvanostatic charge and discharge at a current density of 0.2 A g^{-1}, as shown in Figure 3a. An obvious ultralow discharge plateau at ~0.28 V was observed, which was consistent with the result in CV (Figure 2a). An undesirable low Coulombic efficiency of first cycle <80 % was found as shown in Figure 3a, however, which could be overcome by pre-lithiation technologies during full cell assembling process in LICs. Besides, over 95 % of entire discharge potential was lower than 1.0 V, over 80 % of entire discharge potential was lower than 0.5 V, and ~50 % of entire discharge potential was lower than 0.3 V, which displayed its ultralow potential characterization in comparison with LTO anode.[18] Apart from the discharge potential, we could also obtain that the displayed discharge specific capacity of 3DC@LTSO is over 300 mAh g^{-1}, much higher than the theoretical specific capacity of LTO (170 mAh g^{-1}). These results indicate the 3DC@LTSO with a low discharge potential coupled with a high specific capacity could offset the drawbacks of LTO in a large degree.

Multi-rate performance of 3DC@LTSO and LTSO at the charge and discharge current densities of 0.2~4.0 A g^{-1} was conducted to evaluate their high-rate performance as an anode material (Figure 3c-3d, Figure S4). 3DC@LTSO electrodes displayed a qualitative upgrade in comparison with LTSO electrodes at all charge-discharge rates as shown in Figure S4. In particular, 3DC@LTSO electrodes delivered a high specific capacity of 350 mAh g^{-1} at the current density of 0.2 A g^{-1} and 80 mAh g^{-1} retention was achieved at a high current density of 4.0 A g^{-1} (corresponding to the rate over 20 C for LTO), indicating excellent high-rate performance as an anode material. Moreover, when the current density returned to a low current density of 0.2 A g^{-1}, a relatively high specific capacity of 280 mAh g^{-1} was recovered. Although this specific capacity revealed a decrease in comparison with those in first 20 cycles, the capacity became more stable, indicating a high stability of 3DC@LTSO electrode. Another phenomenon observed was that there was some capacity increase at the first several cycles and the charge and discharge profiles in multi-rate performance tests were different from those of first two cycles. That was mainly ascribed to the amorphization and pulverization of the particles as reported before.[26]

In order to further demonstrate the long-term stability of 3DC@LTSO, the cell was measured under a current density of 2.0 A g^{-1} for up to 3,000 cycles, as shown in Figure 3e. Similar to commonly

Journal of Materials Chemistry A

ARTICLE

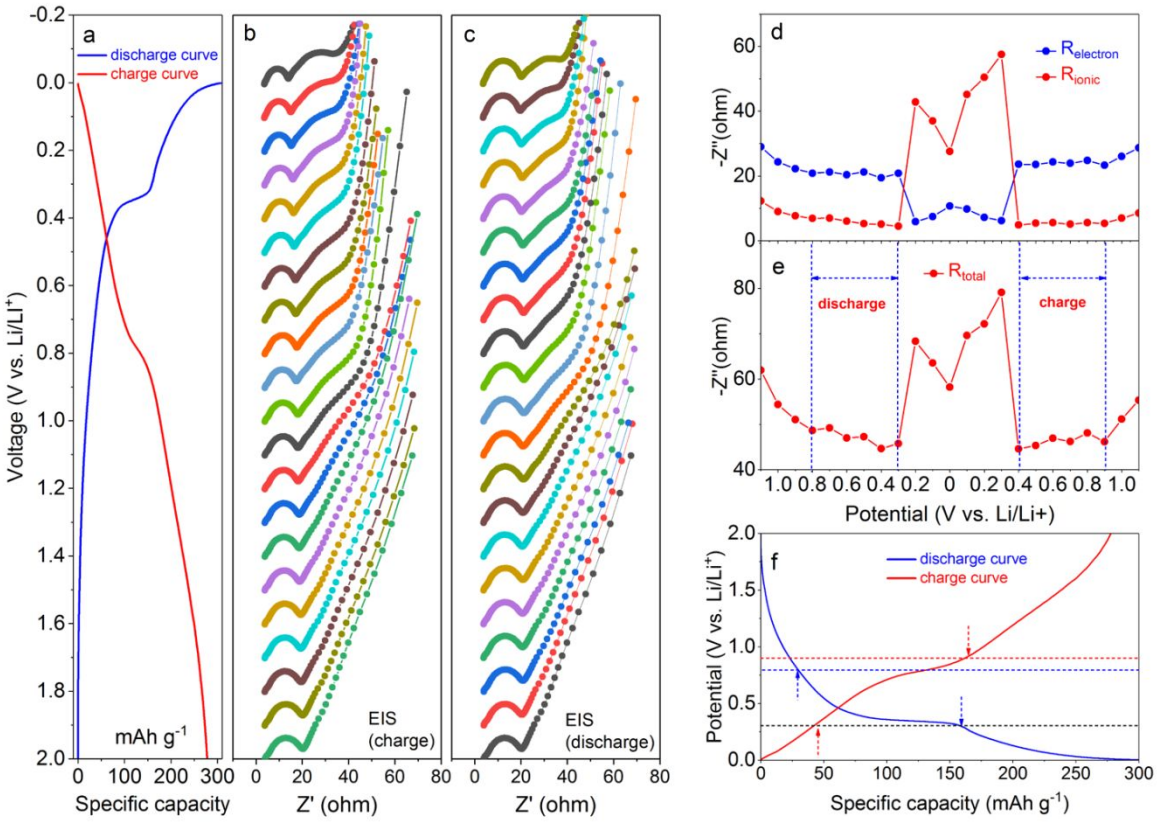

Figure 6. (a) Charge-discharge profile; (b-c) Charge-discharge EIS at different potentials; (d) Quantitative electron transfer and ion diffusion impedance; (e) Total impedance and (f) optimal working potential of 3DC@LTSO electrode.

used electrode materials, the 3DC@LTSO showed a high specific capacity of 150.8 mAh g^{-1} and ultraslow but stable capacity decrease. Nevertheless, after 3,000 cycles, the capacity retention of 3DC@LTSO was still over 80%, indicating totally acceptable long-term cycling stability as anode materials. To now, 3DC@LTSO with the characterizations of the low potential and large specific capacity delivery, as well as outstanding high-rate performance and long cycling lifespan as expectedly, displayed a strong potential as an anode material for LICs.

The cathode material: LDAC

The LDAC was prepared by carbonization-activation process, in which lignin was selected as the precursor and the KOH was used as the activating agent (Figure 4a).[14,15] The structures and morphologies of LDAC were measured by FESEM and TEM. Figure 4b-4c displayed the LDAC with 3D nanoarchitecture, and carbon layer was so thin that the ion will diffuse very fast in LDAC. The TEM images (Figure 4d-4e) revealed that no obvious pore over 50 nm could be observed, indicating no macroporous existing in LDAC.

The porosities and surface structures of the LDAC were investigated by N_2 adsorption-desorption and XPS measurements. As shown in the insertion of Figure 4f, N_2 adsorption-desorption isotherm of the LDAC was ascribed to typical type I isotherms according to IUPAC classification, indicating there were only micropores in LDAC. When the weight ratio of KOH to lignin was adjusted to 1.5:1, the LDAC displayed a largest specific surface area up to 2,808 $m^2 g^{-1}$ with a pore distribution of 0.2~3 nm (Figure 4f), much higher than LDAC with other weight ratio of KOH to lignin (Table S2). The lower weight ratio of KOH to lignin will result in insufficient activation and higher weight ratio of KOH to lignin will results in pore structure collapse, which both lead to lower specific surface area.[38] The mesopores volume in LDAC was negligible and the large micropores structure was capable to deliver high capacitance. Elemental composition of LDAC was shown in Table S1 and O content in LDAC was determined to be 5.8 wt% and 3.85

Journal of Materials Chemistry A

ARTICLE

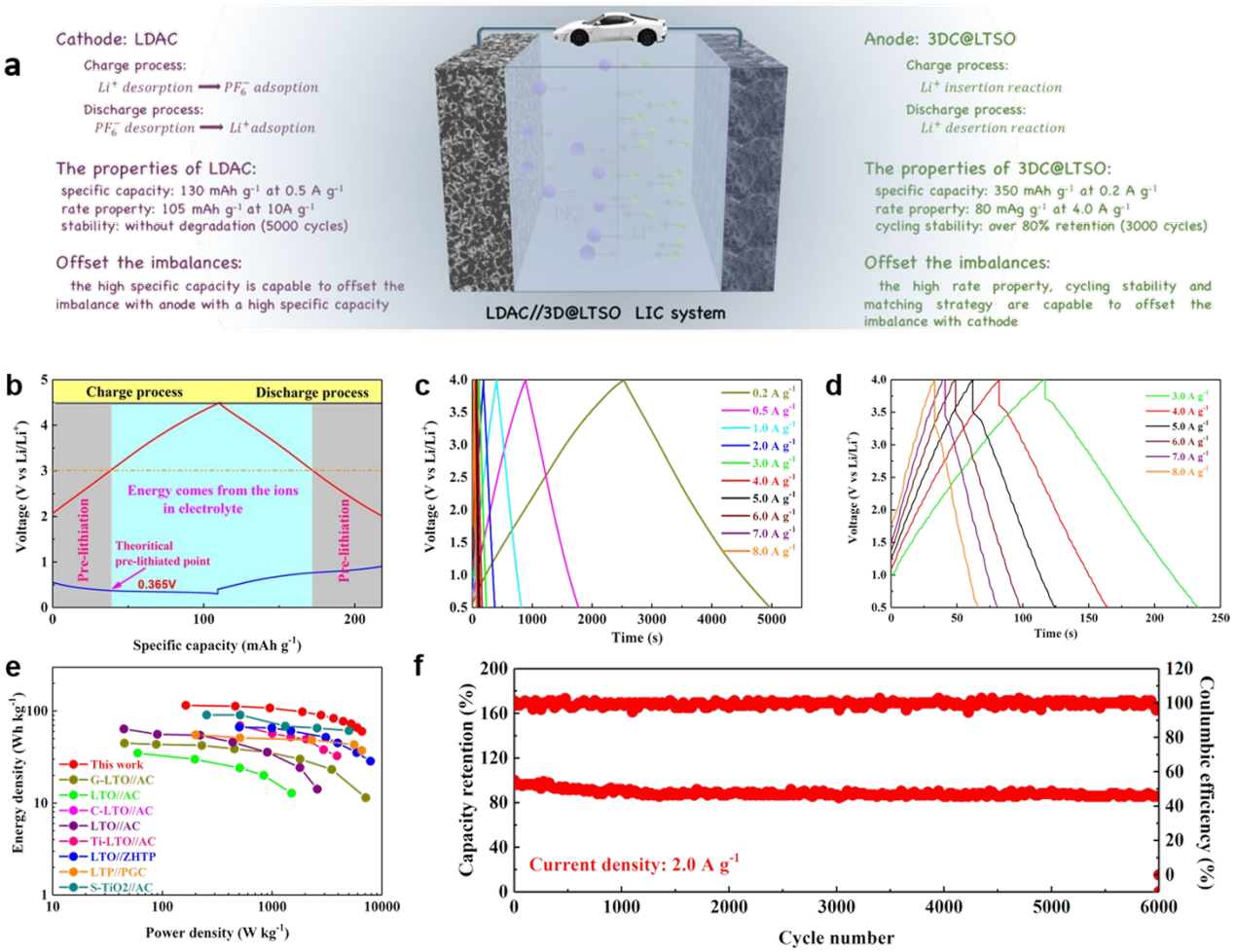

Figure 7. (a) System scheme; (b) Matching scheme; (c-d) Charge-discharge profiles; (e) Ragone plot and (f) Long term cycling stability of LDAC//3DC@LTSO LIC full cell.

wt% by XPS and Elemental Analysis, respectively. And there are 2.3 wt% H and 0.45 wt% N to be detected by Elemental Analysis, too. From the XPS survey spectrum (Figure 4g-4h), the LDAC showed a predominant C 1s peak at 284.15 eV and O 1s peak at 532.20 eV. According to higher binding energies for the C 1s peak, it can be assumed that some carbon atoms were connected to O heteroatoms. The deconvolution of C 1s revealed that there were C=C (284.15 ev), C-C/C-O-C (285 ev), C=O (286.2 ev), and O-C=O (289.8 ev), as shown in Figure 4g. The O 1s peak can be devonvoluted into three peaks at 533.2, 532.2 and 531.2 ev, corresponding to O-C=O, O-C, and O=C peaks.[14,15] The O doping the carbon can play a crucial role in enhancing the local electron density for higher specific capacitance.[14]

As illustrated above, LDAC displayed the characterizations of 3D porous network, abundant porosity, and high specific surface area coupled with abundant oxygen atom doping around carbon, which are all beneficial for high specific capacitance as a cathode material. Then, the electrochemical performance of the LDAC electrode in a half cell was measured by CV and galvanostatic charge and discharge within the potential range of 2.0~4.5 V versus Li/Li^+.[23] The CV curves of LDAC electrodes revealed quasi-rectangular shapes with slight humps at all the scan rates, suggesting dominating electrochemical double layer properties and subordinate pseudocapacitance. The CV curves shown in Figure 5a illustrate good repeatability, indicating excellent high first cycling Coulombic efficiency and cycle stability. The multi-rate performance was also demonstrated under different scanning rates as shown in Figure 5b. The CV curves still kept quasi-

rectangular shape even when the scanning rate increased to 40 mV s^{-1}, indicating desirable reaction kinetics, similar to common activated carbon materials. Same conclusions can also be obtained by galvanostatic charge and discharge as shown in Figure 5c. The linear charge and discharge curves were observed indicating cation and/or anion adsorption-desorption processes. In particular, the LDAC displayed a relatively high capacity of 130 mAh g^{-1} at the current density of 0.5 A g^{-1}, superior rate capability of 105 mAh g^{-1} at 10 A g^{-1} and excellent cycling stability (without any degradation after 5,000 cycles). These properties of LDAC were better than most reported conventional AC or other carbons, displaying strong potential to be a promising cathode material for LICs.

Electrodes matching: 3DC@LTSO with LDAC

The electrochemical performances of as-prepared 3DC@LTSO and LDAC were symmetrically evaluated above. Obviously, by developing excellent high-rate performance and cycling lifespan anode coupled with high specific capacity cathode, the imbalances in specific capacity, high rate behavior, and long cycling lifespan between the two electrodes have been largely alleviated but still existed. Under this circumstance, we attempted to comprehensively evaluate the charge and discharge properties of 3DC@LTSO and selectively utilize optimal profiles with excellent reaction kinetic properties of 3DC@LTSO to match with LDAC cathode.

In this context, we considered to use quasi-in-situ EIS technology to analyse the reaction kinetics of 3DC@LTSO at various charge-discharge potentials (Figure 6a-6c). The constantly changing EIS curves with the reaction undergoing could mainly be divided into two semicircles and a straight line, which corresponded to impedance of SEI, impedance of electron transfer and impedance of ion diffusion process, respectively. In order to quantificationally investigate the electronic and ionic kinetic features, the spectroscopies were fitted by a simplified equivalent circuit, as shown in Figure S7. In particular, the electron transfer impedance, ion diffusion impedance and total impedance were obtained (Figure 6d-6e, Table S3). The impedance characteristics were well correlated with the charge-discharge process (i.e. insertion reaction, conversion reaction, and insertion reaction):[25,26]

$$Li_2^{4d}TiSiO_5 + xLi \leftrightarrow Li_2^{4d}Li_x^{4e}TiSiO_5 \ (x\leq 0.5,\ 3 \text{ to } 0.28\ V) \quad (5)$$

$$Li_2^{4d}Li_x^{4e}TiSiO_5 + (2 - x)\ Li \leftrightarrow Li_4SiO_4 + TiO \ (\text{from } 0.28 \text{ to } >0.1\ V) \quad (6)$$

$$TiO + yLi \leftrightarrow LiyTiO \ (<0.1\ V) \quad (7)$$

During every conversion point at 0.28 and 0.1 V, the impedance characteristics displayed a sudden change as shown in Figure 6d. It could be concluded that the electron transfer impedances of conversion reaction were lower than those of ion diffusion process, while the ion diffusion resistance of conversion reaction were much higher than those of insertion reactions. Therefore, the lowest electrochemical impedances were located in the range of 0.8~0.3 V for discharge and 0.4~0.9 V for charge process (Figure 6f), which indicates the best reaction kinetic properties of 3DC@LTSO in this voltage range. Under this circumstance, a high-performance LIC could be assembled by matching this voltage range of 3DC@LTSO with LDAC cathode.

Lithium ion capacitor: LDAC// 3DC@LTSO

The LIC was fabricated by an LDAC cathode, a 3DC@LTSO anode, and operated in 1M $LiPF_6$ in EC-DMC electrolyte solution, where LDAC underwent an adsorption and desorption process and 3DC@LTSO underwent a lithium insertion and desertion process to achieve energy storage and conversion (Figure 7a). The match scheme of LDAC and 3DC@LTSO was displayed in Figure 7b. Considering the charge and discharge principles of LIC, the optimal pre-lithiated point was determined to 0.365 V. Finally, the LIC was assembled with the same weight of cathode and anode, meanwhile operated in the range of 0.5~4.0 V due to the large over-potential of anode when working at fast charge process (Figure 7c-7d, Figure S8). By this special design, the LIC full cell was unexpectedly capable to charge and discharge at a current density of 8.0 A g^{-1}, two times higher than that in half cells, and an unexpected cycling stability at current density of 2.0 A g^{-1} was obtained with over 90 % retention after 6,000 cycles (Figure 7c and 7f), much more stable than that in half cells. Benefited from the effective match approach, the high-rate performance and cycling stability of 3DC@LTSO anode in full cells were both surprisingly better than those in half cell evaluation, indicating the match process further offset the imbalances between two electrodes for improvement of the performance of LICs.

The Ragone plot (energy density vs. power density) of LDAC//3DC@LTSO full cell was shown in Figure 7e. As expected, the assembled LDAC//3DC@LTSOC showed a high-energy density of 115.3 Wh kg^{-1} at 163.5 W kg^{-1} and a high-power density of 6,560 W kg^{-1} at 60 Wh kg^{-1} (all the data was based on the total weight of cathode and anode active materials). The values reached by the LDAC//3DC@LTSO were higher than those of reported LTO based LIC system (Figure 7e, details in Table S4).[39–46] These results proved LDAC//3DC@LTSO system was a promising energy storage device which combined high energy density and long cycling lifespan.

Conclusions

A high energy-density and long cycling-lifespan LIC assembled by a 3D carbon modified LTSO (3DC@LTSO) anode and a lignin-derived activated carbon (LDAC) cathode was designed and fabricated. 3D carbon structure with interlaced electron and ion diffusion channels enabled LTSO to have a large Li-ion storage capacity (>350 mAh g^{-1}), an acceptable charge and discharge rate (~ 4.0 A g^{-1}) as well as a stable life durability (>3000 cycles) within a low working window from 0.005 to 2.0 V (vs. Li/Li^+), satisfying the demands for applications in LICs. Meanwhile, LDAC was synthesized by a directly carbonization-activation process. The LDAC was capable to deliver a high specific capacitance (>110 mAh g^{-1}) due to following favorable microstructural characteristics: (*i*) 3D porous network; (*ii*) abundant porosity; (*iii*) high specific surface area (2,808 m^2 g^{-1}). These two desirable electrode materials would much favorably offset the imbalances in specific capacity and high-rate performance between two electrodes. Moreover, a novel electrodes-matching strategy, which was capable to further offset the imbalance between two electrodes (including high-rate performance and cycling lifespan), was proposed and applied into this system, symmetrically. Thereby, the assembled LDAC//3DC@LTSO cell showed a high energy density of 115.3 Wh kg^{-1} at 163.5 W kg^{-1} and a high-power density of 6,560 W kg^{-1} at 60 Wh kg^{-1}, coupled with an excellent cycling lifespan of 90% capacity retention after 6,000 cycles at the current density of

2.0 A g^{-1}. These excellent results were promising in terms of pushing high energy-density and long-cycling lifespan LIC by tailoring the nanostructures of both electrodes and optimizing the electrode-matching strategic approaches.

Conflicts of interest

There are no conflicts to declare.

Acknowledgements

The authors acknowledge the financial support from the National Natural Science Foundation of China, Grant Nos. 51777140, and the Fundamental Research Funds for the Central Universities at Tongji University No. 2212018030 and No. 22120180519. And also, this work was partly supported by US Army Research Laboratory under contract No. W911NF-12-R-0011-03.

Notes and references

1 W. A. Braff, J. M. Mueller and J. E. Trancik, *Nature Climate Change*, 2016, **6**, 964–969.
2 N. Kittner, F. Lill and D. M. Kammen, *Nature Energy*, 2017, **2**, 17125.
3 N.-S. Choi, Z. Chen, S. A. Freunberger, X. Ji, Y.-K. Sun, K. Amine, G. Yushin, L. F. Nazar, J. Cho and P. G. Bruce, *Angewandte Chemie International Edition*, 2012, **51**, 9994–10024.
4 Y. Wang, Y. Song and Y. Xia, *Chemical Society Reviews*, 2016, **45**, 5925–5950.
5 F. Wang, X. Wu, X. Yuan, Z. Liu, Y. Zhang, L. Fu, Y. Zhu, Q. Zhou, Y. Wu and W. Huang, *Chemical Society Reviews*, 2017, **46**, 6816–6854.
6 L. Zhou, K. Zhang, Z. Hu, Z. Tao, L. Mai, Y.-M. Kang, S.-L. Chou and J. Chen, *Advanced Energy Materials*, 2018, **8**, 1701415.
7 A. Manthiram, *ACS Cent. Sci.*, 2017, **3**, 1063–1069.
8 S. Xin, Y. You, S. Wang, H.-C. Gao, Y.-X. Yin and Y.-G. Guo, *ACS Energy Lett.*, 2017, **2**, 1385–1394.
9 Y. Zhai, Y. Dou, D. Zhao, P. F. Fulvio, R. T. Mayes and S. Dai, *Advanced Materials*, 2011, **23**, 4828–4850.
10 R. R. Salunkhe, Y.-H. Lee, K.-H. Chang, J.-M. Li, P. Simon, J. Tang, N. L. Torad, C.-C. Hu and Y. Yamauchi, *Chemistry – A European Journal*, 2014, **20**, 13838–13852.
11 B. Li, J. Zheng, H. Zhang, L. Jin, D. Yang, H. Lv, C. Shen, A. Shellikeri, Y. Zheng, R. Gong, J. P. Zheng and C. Zhang, *Advanced Materials*, 2018, **30**, 1705670.
12 H. Wang, C. Zhu, D. Chao, Q. Yan and H. J. Fan, *Advanced Materials*, 2017, **29**, 1702093.
13 H. Wang, Y. Zhang, H. Ang, Y. Zhang, H. T. Tan, Y. Zhang, Y. Guo, J. B. Franklin, X. L. Wu, M. Srinivasan, H. J. Fan and Q. Yan, *Advanced Functional Materials*, 2016, **26**, 3082–3093.
14 B. Li, F. Dai, Q. Xiao, L. Yang, J. Shen, C. Zhang and M. Cai, *Advanced Energy Materials*, 2016, **6**, 1600802.
15 B. Li, F. Dai, Q. Xiao, L. Yang, J. Shen, C. Zhang and M. Cai, *Energy & Environmental Science*, 2016, **9**, 102–106.
16 S. R. Sivakkumar and A. G. Pandolfo, *Electrochimica Acta*, 2012, **65**, 280–287.
17 S. R. Sivakkumar, J. Y. Nerkar and A. G. Pandolfo, *Electrochimica Acta*, 2010, **55**, 3330–3335.
18 K. Naoi, *Fuel Cells*, 2010, **10**, 825–833.
19 K. Naoi, S. Ishimoto, Y. Isobe and S. Aoyagi, *Journal of Power Sources*, 2010, **195**, 6250–6254.
20 G. Wang, C. Lu, X. Zhang, B. Wan, H. Liu, M. Xia, H. Gou, G. Xin, J. Lian and Y. Zhang, *Nano Energy*, 2017, **36**, 46–57.
21 S. Zhang, C. Li, X. Zhang, X. Sun, K. Wang and Y. Ma, *ACS Appl. Mater. Interfaces*, 2017, **9**, 17136–17144.
22 R. Yi, S. Chen, J. Song, M. L. Gordin, A. Manivannan and D. Wang, *Advanced Functional Materials*, 2014, **24**, 7433–7439.
23 L. Shen, H. Lv, S. Chen, P. Kopold, P. A. van Aken, X. Wu, J. Maier and Y. Yu, *Advanced Materials*, 2017, **29**, 1700142.
24 E. Iwama, N. Kawabata, N. Nishio, K. Kisu, J. Miyamoto, W. Naoi, P. Rozier, P. Simon and K. Naoi, *ACS Nano*, 2016, **10**, 5398–5404.
25 J. Liu, W. Kong Pang, T. Zhou, L. Chen, Y. Wang, V. K. Peterson, Z. Yang, Z. Guo and Y. Xia, *Energy & Environmental Science*, 2017, **10**, 1456–1464.
26 J. Liu, Y. Liu, M. Hou, Y. Wang, C. Wang and Y. Xia, *Electrochimica Acta*, 2018, **260**, 695–702.
27 R. Agrawal, C. Chen, S. Dages and C. Wang, *Advanced Materials Letters*, 2017, **8**, 783–790.
28 H. Wang, T. Liang, D. Xu, K. Liao, Y. Gong, R. Wang, B. He and C. Yan, *Nanoscale*, , DOI:10.1039/C8NR04292F.
29 J. Ajuria, M. Arnaiz, C. Botas, D. Carriazo, R. Mysyk, T. Rojo, A. V. Talyzin and E. Goikolea, *Journal of Power Sources*, 2017, **363**, 422–427.
30 J. Jiang, P. Nie, B. Ding, Y. Zhang, G. Xu, L. Wu, H. Dou and X. Zhang, *Journal of Materials Chemistry A*, 2017, **5**, 23283–23291.
31 F. Sun, X. Liu, H. B. Wu, L. Wang, J. Gao, H. Li and Y. Lu, *Nano Lett.*, 2018, **18**, 3368–3376.
32 C. Rodríguez, M. Stollovsky, T. Hehr, Y. Rauscher, B. Rolli, and A. Kruse, 2017, **9**, 8222-8233.
33 E. Atta-Obeng, B. Dawson-Andoh, M. S. Seehra, U. Geddam, J. Poston and J. Leisen, *Biomass and Bioenergy*, 2017, **107**, 172–181.
34 P. Yu, G. Cao, S. Yi, X. Zhang, C. Li, X. Sun, K. Wang and Y. Ma, *Nanoscale*, 2018, **10**, 5906–5913.
35 W. Cai, G. Li, F. He, L. Jin, B. Liu and Z. Li, *Journal of Power Sources*, 2015, **283**, 524–529.
36 L. M. Jin, F. He, W. L. Cai, J. X. Huang, B. H. Liu and Z. P. Li, *Journal of Power Sources*, 2016, **328**, 536–542.
37 B. Wang, T. Liu, A. Liu, G. Liu, L. Wang, T. Gao, D. Wang and X. S. Zhao, *Advanced Energy Materials*, 2016, **6**, 1600426.
38 J. Wang and S. Kaskel, *Journal of Materials Chemistry*, 2012, **22**, 23710–23725.
39 C. Lu, X. Wang, X. Zhang, H. Peng, Y. Zhang, G. Wang, Z. Wang, G. Cao, N. Umirov and Z. Bakenov, *Ceramics International*, 2017, **43**, 6554–6562.
40 K. Naoi, S. Ishimoto, Y. Isobe and S. Aoyagi, *Journal of Power Sources*, 2010, **195**, 6250–6254.
41 L. Wang, H. Yang, T. Shu, Y. Xin, X. Chen, Y. Li, H. Li and X. Hu, *ACS Appl. Energy Mater.*, 2018, **1**, 1708–1715.
42 X. Zhang, C. Lu, H. Peng, X. Wang, Y. Zhang, Z. Wang, Y. Zhong and G. Wang, *Electrochimica Acta*, 2017, **246**, 1237–1247.
43 S. Dong, X. Wang, L. Shen, H. Li, J. Wang, P. Nie, J. Wang and X. Zhang, *Journal of Electroanalytical Chemistry*, 2015, **757**, 1–7.
44 C. Kim, N. S. Norberg, C. T. Alexander, R. Kostecki and J. Cabana, *Advanced Functional Materials*, 2013, **23**, 1214–1222.
45 Y. Lei, Z.-H. Huang, Y. Yang, W. Shen, Y. Zheng, H. Sun and F. Kang, *Scientific Reports*, 2013, **3**, 2477.
46 A. Jain, V. Aravindan, S. Jayaraman, P. S. Kumar, R. Balasubramanian, S. Ramakrishna, S. Madhavi and M. P. Srinivasan, *Scientific Reports*, 2013, **3**, 3002.